Molecular Dynamics Study on the Interaction of a Mithramycin Dimer with a Decanucleotide Duplex

Shih-Yuan Chen and Thy-Hou Lin*

Institute of Molecular Medicine and Department of Life Science, National Tsing Hua University, Hsinchu 30013, Taiwan

Received: October 22, 2004; In Final Form: March 10, 2005

The complex of a minor groove binding drug mithramycin (MTR) and the self-complementary d(TAGCTAGCTA) 10-mer duplex was investigated by molecular dynamics (MD) simulations using the AMBER 7.0 suite of programs. There is one disaccharide and trisaccharide segment projecting from opposite ends of an aglycone chromophore of MTR. A MTR dimer complex $(MTR)_2Mg^{2+}$ is formed in the presence of a coordinated ion Mg^{2+}. A NMR solution structure of two $(MTR)_2Mg^{2+}$ complexes bound with one DNA duplex, namely, the 2:1 duplex complex, was taken as the starting structure for the MD simulation. The partial charge on each atom was calculated using the multiple-RESP fitting procedure, and all of the missing parameters in the Parm99 force field used were adapted comparably from the literature. The length of the MD simulation was 5 ns, and the binding free energy for the formation of a 1:1 or 2:1 duplex complex was determined from the last 4 ns of the simulation. The binding free energies were decomposed to components of the contributions from different energy types, and the changes in the helical parameters of the bound DNA duplex plus the glycosidic linkages between sugar residues of the bound MTR dimer were determined. It was found that binding of the first $(MTR)_2Mg^{2+}$ complex with the DNA duplex to form a 1:1 duplex complex does not cause stiffening of the duplex especially in the unoccupied site of the duplex. However, the overall flexibility of the DNA duplex is reduced substantially once the second $(MTR)_2Mg^{2+}$ complex is bound with the unoccupied site to form the 2:1 duplex complex. The van der Waals interactions were found to be dominant in the central part of the DNA duplex where sugar residues from each bound $(MTR)_2Mg^{2+}$ complex were inwardly pointing and the corresponding minor groove was widened.

Introduction

Mithramycin (MTR) is a GC-specific DNA binding antibiotic that inhibits RNA synthesis initiation.[1,2] It inhibits binding of *Escherichia coli* RNA polymerase to a poly dGdC template, but does not inhibit binding to a poly dAdT template.[2] This suggests that MTR may bind to GC-rich sequences in eukaryotic promoters and inhibit RNA synthesis by preventing the binding of regulatory proteins, such as Sp1, to these sites. MTR is also an effective differentiating agent of HL60 promyelocytic leukemia cells as well as the leukemia cells of certain patients with the myeloid blast phase of chronic myelogenous leukemia.[3,4] Expression of the c-myc protooncogene is selectively inhibited by MTR treatment in a number of differentiating and nondifferentiating cell types.[5]

In the presence of a divalent cation such as Mg^{2+}, the antibiotic binds Mg^{2+} to form two different types of antibiotic−Mg^{2+} complexes, complex I (1:1) and complex II (2:1) or $(MTR)Mg^{2+}$ and $(MTR)_2Mg^{2+}$, respectively.[6] These two complexes are different molecular entities as shown by recent spectroscopic and kinetic studies using the high-performance liquid chromatography technique.[9−13] They are the potential DNA binding ligands and bind DNA differently.[11−16] The 2:1 complex binds specifically to the GC region of a DNA minor groove.[16] While there is a steric hindrance presented by the C2 amino group of the guanine base, the deep and narrow B-DNA minor groove is widened for the binding with the $(MTR)_2Mg^{2+}$ ligands.[14,16−18] The base specificity has been ascribed to the formation of hydrogen bonds between potential sites in the guanine base and ligands.[14−16] The binding of the $(MTR)_2Mg^{2+}$ complex to partially overlapping sites on $d(TAGCTAGCTA)_2$, a self-complementary 10-mer duplex, has been investigated by Sastry et al.[19] using the NMR technique. The NMR solution structure shows that two $(MTR)_2Mg^{2+}$ complexes bind with one 10-mer duplex with a stoichiometry of 2:1 or 5−6 nucleotide bases/molecule of MTR.[11,12] The glycosidic linkage bonds along the aglycone-C-D-E trisaccharide segment of $(MTR)_2Mg^{2+}$ are found to be flexible so that two $(MTR)_2Mg^{2+}$ complexes can bind simultaneously with the minor groove that is being opened by a kink at the central T−A/T−A part of the 10-mer duplex.[19] A spectroscopic study on the same $(MTR)_2Mg^{2+}$−DNA duplex complex system has revealed that the association is an enthalpy-driven event.[6]

The molecular dynamics (MD) simulations using an explicit solvent model have been conducted to reliably reproduce varied DNA structure, dynamics, and interactions with some drug molecules.[7,8] A MD simulation on the binding between distamycin and B-DNA oligomer $d(CGCAAATTTGCG)_2$ reveals that binding of the drug with the minor groove induces a stiffening of the DNA helix and prevents a conformational change from B-DNA to A-DNA.[20] The origins of cooperativity in drug−DNA complexes have been investigated using the MD simulation for a minor groove binding drug Hoechst 33258 with the duplex $d(CTTTTCGAAAAG)_2$.[22] In this study, some thermodynamic parameters are computed from a series of MD simulations on the free DNA, 1:1, and 2:1 complexes.[22] The

* Author to whom correspondence should be addressed. Fax: 886-3-571-5934. E-mail: thlin@life.nthu.edu.tw.

10.1021/jp045171v CCC: $30.25
Published on Web 04/15/2005

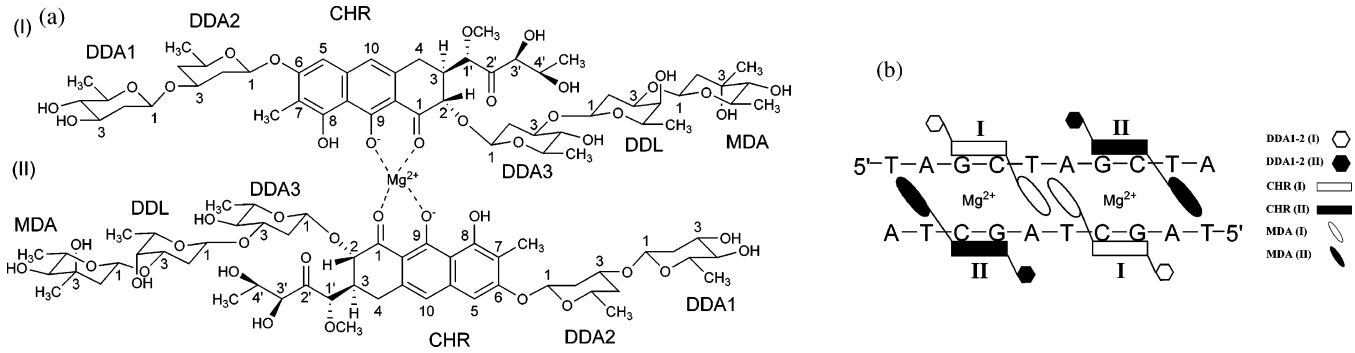

Figure 1. Two-dimensional diagram for (a) the MTR dimer coordinated with Mg^{2+} and (b) the 2:1 $(MTR)_2Mg^{2+}$−DNA duplex complex. The two MTR monomers with respective chain IDs, I and II, are coordinated to the divalent Mg^{2+} ion through the O1 carbonyl and ionized O9 enolate anion on the hydrophilic edge of each aglycone chromophore (CHR). All residues are labeled based on the description in the PDB file ID 207D.

results indicate that the cooperativity observed cannot be ascribed to the enthalpic and hydration factors alone but rather as a combination of the two plus the configuraional entropy computed as well.[22] In this study, we present a MD simulation result of 5 ns for the 1:1 and 2:1 $(MTR)_2Mg^{2+}$−10-mer $d(TAGCTAGCTA)_2$ duplex complexes plus the free $(MTR)_2Mg^{2+}$ complex and free duplex in an explicit water model. The solution structure of the 2:1 $(MTR)_2Mg^{2+}$−10-mer $d(TAGCTAGCTA)_2$ duplex complex determined by NMR by Sastry et al.[19] is taken as the starting structure for the MD simulation. The divalent cation coordination site on the $(MTR)_2Mg^{2+}$ complex has been elucidated by Gao and Patel[23] to be the O1 carbonyl and ionized O9 enolate anion on the hydrophilic edge of each aglycone chromophore (CHR) (Figure 1a). The $(MTR)_2Mg^{2+}$ complex is found to bind with each of the following self-complementary hexanucleotide duplexes: $d(TGGCCA)_2$,[16] $d(TCGCGA)_2$,[17] and $d(TAGCTA)_2$.[17] The DDA3-DDL sugar segment of one MTR shares a widened minor groove with the aglycone of the second MTR while the MDA sugar is directed face-down toward the floor of the minor groove spanning two base pairs in each of these 1:1 $(MTR)_2Mg^{2+}$−6-mer duplex complexes.[17] The MDA sugar remains face-down toward the floor of the minor groove, which is opened substantially by a kink at the central T−A/T−A step to accommodate the inwardly pointing MDA sugars from the second $(MTR)_2Mg^{2+}$ complex bound to the adjacent site (Figure 1b) in the structure of the 2:1 $(MTR)_2Mg^{2+}$−10-mer $d(TAGCTAGCTA)_2$ duplex complex where the duplex is made by two partially overlapping 6-mer binding sites.[19] We compute free energies for binding of the drug with the DNA duplex using the molecular mechanics (MM) generalized Born surface area (GB-SA) approach[24] implemented in the AMBER 7.0 package.[25] In this approach, the gas-phase energies, solvation free energies, and entropic contributions are summed and averaged over snapshots from the MD trajectories. The binding free energies computed are decomposed to components contributed from different interaction types on a per residue basis. We also compare the DNA helical parameters and glycosidic torsion angles of all the sugar residues in the $(MTR)_2Mg^{2+}$ complex for the free DNA duplex, 1:1, and 2:1 duplex complexes during the binding process. The difference in binding between one or two $(MTR)_2Mg^{2+}$ complexes with the DNA duplex to form a 1:1 or 2:1 duplex complex is explored using both the energy and the geometric data computed.

Materials and Methods

The MD simulation was performed using the AMBER 7.0 suite of programs.[25] The Parm99[26]/TIP3P[27] force field was used to parametrize the DNA and solvent. The charges of $(MTR)_2Mg^{2+}$, the MTR dimer coordinated by Mg^{2+}, were calculated using the HF/6-31G(d)/RESP method[28] and were fitted by the multiple conformation RESP approach. The structures of (I) MTR−Mg^{2+}, (II) two CHR residues coordinated by Mg^{2+}, and (III) both disaccharide and trisaccharide residues of MTR were optimized, and the corresponding electrostatic potentials were calculated at the HF/6-31G(d) level of theory. The partial charges on each atom were then deduced through the multiple RESP fitting by specifying additional molecule atom equivalence between these molecules. The Glycam2000 force field parameters developed by Woods et al.[29] were used to describe the sugar residues of MTR. The Parm99 force field parameters were used to describe the CHR residue, and the missing parameters for joints between the CHR and sugar residues were adapted from comparable parameters.

The MD simulations in explicit water models were performed for the following systems: 2:1 $(MTR)_2Mg^{2+}$−DNA duplex complex, 1:1 $(MTR)_2Mg^{2+}$−DNA duplex complex, free DNA, and $(MTR)_2Mg^{2+}$ alone. The starting structure of the 2:1 duplex complex was taken as the NMR-derived one. The stripped structures from the 2:1 NMR-derived one were taken as the starting structures for the other systems. The number of TIP3P waters placed in a periodic box for solvating the 2:1 and 1:1 duplex complexes, free DNA, and the free $(MTR)_2Mg^{2+}$ complex were 3440, 3106, 2686, and 1893, respectively. There were 18 sodium ions used as counterions, and they were added by the LEAP module to each system to maintain the electroneutrality. The particle mesh Ewald (PME) method[30] was used to account for the long-range electrostatic interactions, and all of the bonds between the hydrogen atoms and the heteroatoms were constrained by the SHAKE algorithm.[31]

To equilibrate all of the systems, energy minimization by 200 steps of steepest descent followed by 800 steps of conjugate gradient minimization was conducted. A harmonic restraint of 10 kcal/(mol Å^2) was imposed on solutes while heating and equilibrating the systems. Each system was gradually heated from 0 to 300 K within 60 ps by a constant volume MD simulation. A constant pressure MD simulation at 300 K for 60 ps was subsequently performed to ensure all of the solutes were well-solvated. Each system was equilibrated for 60 ps by a constant pressure MD simulation to gradually reduce the corresponding force constant to 0.2 kcal/(mol Å^2). The final equilibrated structures were subjected to production dynamics of 5 ns at 300 K where no harmonic restraints were imposed. The time constants for heat bath coupling and pressure relaxation were both set as 2.0 ps in the period of production dynamics. The translational motion of the center-of-mass was removed every 5 ps during the 5 ns dynamics.

The root-mean-square deviations (rmsd's) of the final structures from the starting ones were computed by the PTRAJ

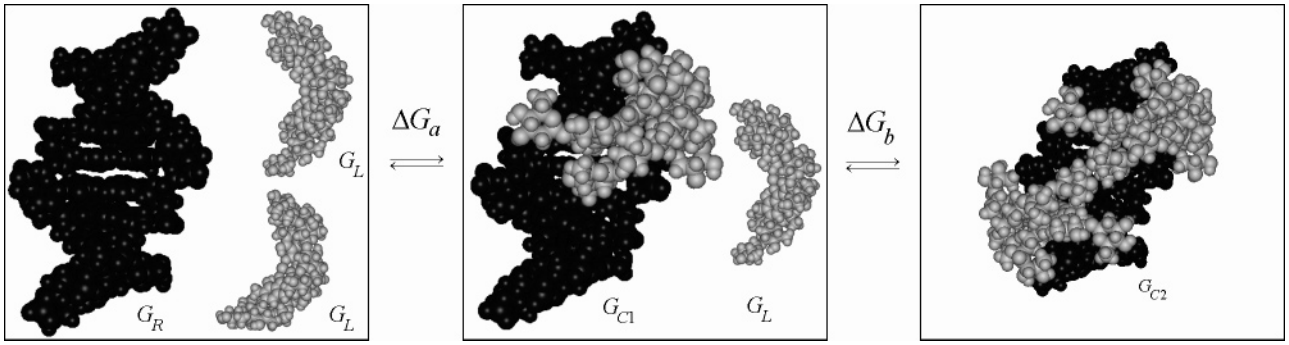

Figure 2. Thermodynamics cycle used for calculating the binding free energy and some related parameters during the binding process. G_R is the free energy of the free DNA duplex, G_L is the free energy of the free $(MTR)_2Mg^{2+}$ complex, G_{C1} is the free energy of the 1:1 $(MTR)_2Mg^{2+}$ duplex complex, and G_{C2} is the free energy of the 2:1 $(MTR)_2Mg^{2+}$ duplex complex. $\Delta G_a = (G_{C1} + G_L) - (G_R + 2G_L)$, $\Delta G_b = G_{C2} - (G_{C1} + G_L)$, and $\Delta\Delta G = \Delta G_b - \Delta G_a = G_{C2} + G_R - 2G_{C1}$.

module of AMBER. The minor groove widths of each DNA structure were analyzed using the Curves5 program.[32] The thermodynamics cycle depicted in Figure 2 was used to compute the binding free energies for the 1:1 and 2:1 $(MTR)_2Mg^{2+}$–10-mer $d(TAGCTAGCTA)_2$ duplex complexes. This putative scheme was derived from the NMR experiment.[19] The binding free energy for each $(MTR)_2Mg^{2+}$ complex bound with the 10-mer DNA duplex was computed as follows

$$G = E_{gas} + G_{solv} - TS_{conf} \quad (1)$$

where E_{gas} was the gas-phase energy, G_{solv} was the solvation free energy, and S_{conf} was the configurational entropy determined by normal-mode analysis. For each simulation, 4000 snapshots for each being 1 ps long and without solvent molecules were taken from the last 4 ns dynamics to calculate the gas-phase and implicit solvation contributions, and 800 snapshots without solvent molecules for every 5 ps each were taken from the same period to calculate entropy contributions. The bond, angle, dihedral, Lennard-Jones, and Coulombic energies computed were summed up as the gas-phase energies. The solvation free energies were computed using the GB model developed by Tsui and Case.[24] The hydrophobic contribution to the solvation free energy and the implicit solvation free energy were computed from the solvent-accessible area (SA) by Paul Beroza's Molsurf module of AMBER. In brief, the MM/GB-SA approach was used to estimate the $E_{gas} + G_{solv}$ terms in eq 1. The salt concentration for calculating the generalized Born energy was set as 0.1 M, corresponding to the buffer concentration described in the NMR study.[19] The translational and rotational entropy were calculated as those described by McQuarrie[33] while the vibrational entropy was calculated by a normal-mode analysis via the Nmode module of AMBER.

To compute the vibrational entropy through normal-mode analysis, each structure of the snapshots was minimized by a conjugate gradient method until a convergence criterion of 10^{-4} kcal/(mol Å) was reached, and then the frequency of the vibrational modes was computed at 300 K with a distance-dependent dielectric of $4r$ where r was the distance between two atoms. The quasiharmonic normal-mode analysis was performed for each half of the DNA duplex extracted from the free DNA, 1:1 and 2:1 duplex complexes, also for $(MTR)_2Mg^{2+}$ extracted from the free $(MTR)_2Mg^{2+}$, and 1:1 and 2:1 duplex complexes by calculating the mass-weighted covariance matrix from the MD snapshots via the PTRAJ8 module of AMBER8 to compare the change in configurational entropy upon binding with the drug and DNA, respectively. The top eigenvector was computed from the MD trajectories, and harmonic modes of the free DNA were generated corresponding to the maximum and minimum of eigenvalues computed by the PTRAJ8 module. All calculations were performed on an IBM P690 cluster and our in-lab PC equipped with an Intel Pentium4 processor.

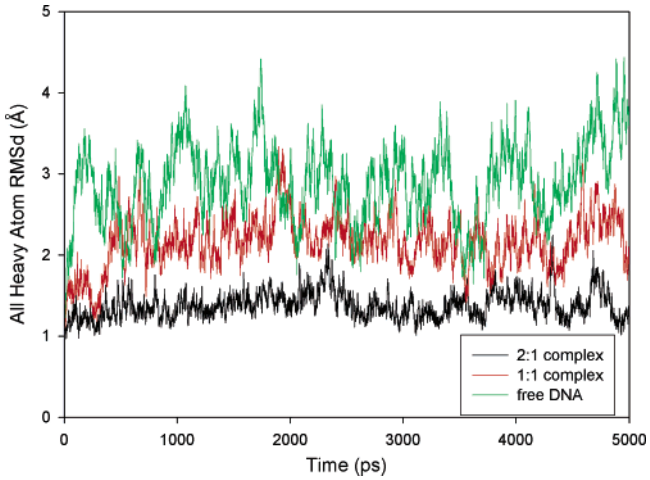

Figure 3. Root-mean-squared deviation (rmsd) values of the coordinates of all of the heavy atoms of the 1:1 and 2:1 duplex complexes and the free DNA from those of the starting NMR structure plotted against the simulation time during the 5 ns MD simulation.

Results and Discussion

The progress of MD simulation results are examined by comparing the rmsd values of the coordinates of all heavy atoms generated over the 5 ns MD simulation with those of the corresponding NMR structure as presented in Figure 3. The difference between NMR and the averaged rmsd values of MD-derived structures over the trajectory computed for the 1:1 and 2:1 duplex complexes and free DNA are 1.38, 2.16, and 2.88 Å, respectively (Figure 3). Apparently, the structures generated by the MD simulation for the 2:1 duplex complex are in good agreement with the corresponding NMR one, suggesting that the force field parameters used in the MD simulation are adequate. The DNA duplex appears to be flexible during the MD simulation since a substantial fluctuation in the rmsd values is computed for both the 1:1 duplex complex and the free DNA. The $(MTR)_2Mg^{2+}$ complex appears to be more flexible in the unbound than in the bound state (Table 1). However, the averaged structure of the 2:1 duplex complex obtained from the MD simulation superimposes well on the corresponding NMR structure as shown in Figure 4.

The helical parameters of DNA duplexes of 1:1 or 2:1 duplex complexes obtained from the 5 ns MD simulation are compared with those computed for the corresponding NMR structure as

TABLE 1: Root-Mean-Squared Deviation of Coordinates of $(MTR)_2Mg^{2+}$ and DNA to Their Average Structures from the Nonbound, 1:1, and 2:1 Complexes[a]

	$(MTR)_2Mg^{2+}$		DNA	
system	average	deviation	average	deviation
nonbound	3.17	0.34	1.67	0.41
1:1 complex	1.14	0.25	1.64	0.30
2:1 complex	0.98[b]	0.24[b]	1.14	0.17

[a] All values are in angstroms and are calculated over 4000 snapshots from the separate MD simulations (1.0−5.0 ns). [b] Averaged from rmsd values of 0.96 and 0.99, averaged from rmsd values of 0.22 and 0.26 for two $(MTR)_2Mg^{2+}$ complexes.

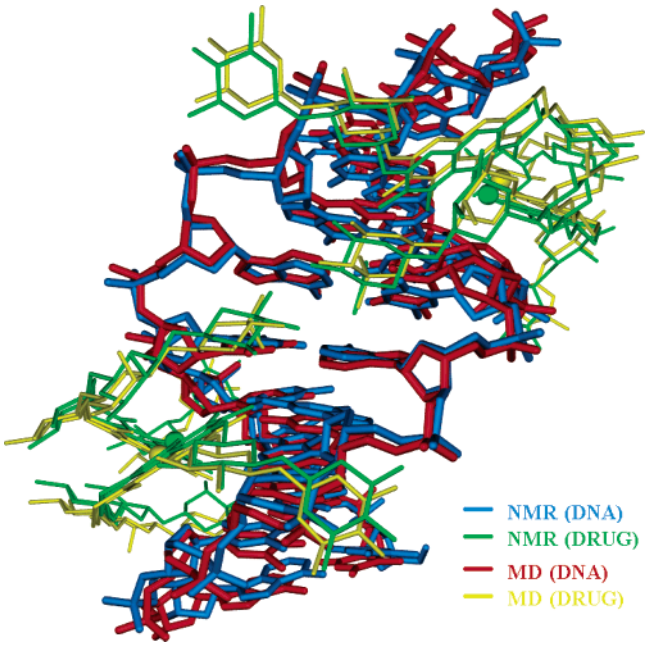

Figure 4. Superposition of the averaged structures of the 2:1 duplex complex obtained from the 5 ns MD simulation on the NMR starting structure. The hydrogen atoms and hydrophilic chains of the CHR residues of each $(MTR)_2Mg^{2+}$ complex are not shown for brevity.

shown in Figure 5. For the 2:1 duplex complex, all of the helical parameters computed for the structures obtained from the MD simulation appear to be in accord with those computed for the corresponding NMR structure (Figure 5). However, all of the helical parameters computed for the 1:1 duplex complex are quite different from those computed for both the 2:1 duplex complex and the NMR structure (Figure 5). There is an apparent transition in the helical rise or twist at the T5−A6 step beyond which the 1:1 duplex is unoccupied (Figures 5a and 5b). The transition in both helical parameters observed may be caused by the interaction between the T5 and A6 bases. The computed minor groove widths, the available spaces for drug binding, are compared in Figure 5c for both the 1:1 and 2:1 duplex complexes and the NMR structure. While values of the minor groove widths computed for both the 2:1 duplex complex and the NMR structure agree well with each other and are symmetrical with respect to the central overlapping region, those computed for the 1:1 duplex complex deviate substantially from the T5−A6 step to the end where the duplex is unoccupied (Figure 5c).

The change in conformation for the free and bound $(MTR)_2Mg^{2+}$ complex of 1:1 or 2:1 duplex complexes during the 5 ns MD simulation is inspected by comparing the averaged glycosidic torsion angles measured and is presented in Figures 6a and 6b. Each of the MTR monomers in a $(MTR)_2Mg^{2+}$ complex is labeled as monomer I and II, respectively (Figure

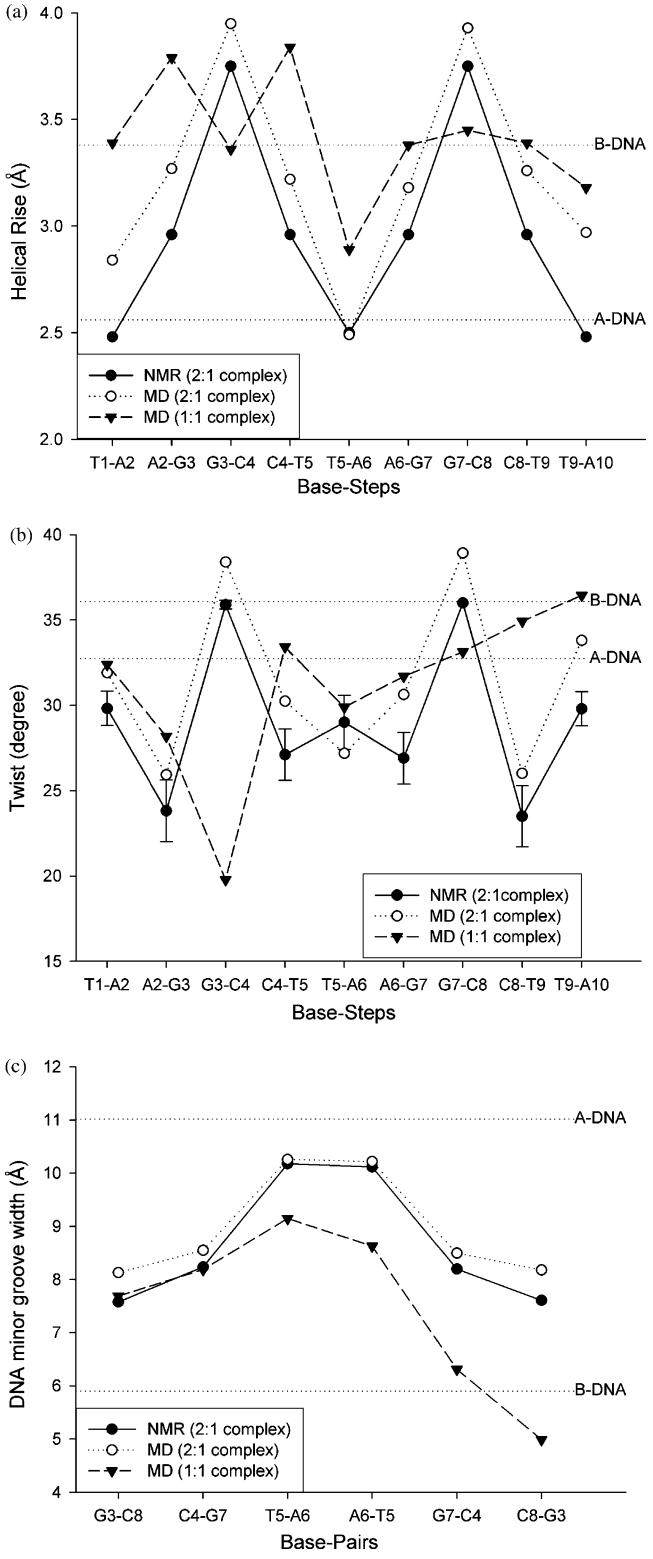

Figure 5. DNA helical parameters calculated for the time-averaged structures of the 1:1 and 2:1 duplex complexes and the starting NMR structure: (a) the helical rise at individual base step, (b) the helical twist at an individual base step (with deviation bars drawn for the NMR set) in each duplex complex, and (c) DNA minor groove widths at each base pair.

1). In general, most of the glycosidic linkages of structures of the 2:1 duplex complex generated by the MD simulation agree plausibly with those of the NMR-derived one (Figure 6a). No difference between each glycosidic torsion angle of either monomer I or II of the two $(MTR)_2Mg^{2+}$ complexes bound in the 2:1 duplex complex is observed, indicating that these two

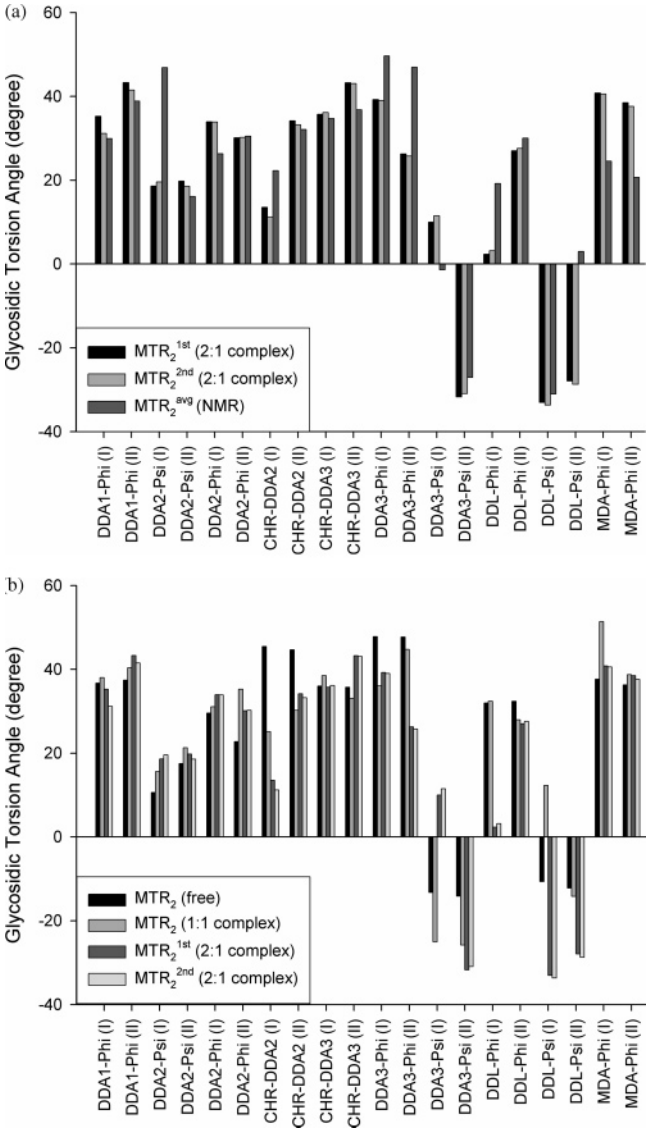

Figure 6. (a) Glycosidic torsion angles of all of the sugar residues of the bound $(MTR)_2Mg^{2+}$ complex in a 2:1 duplex complex determined from the 5 ns dynamics simulation plus those determined for the NMR structure. (b) The glycosidic torsion angles of all of the sugar residues of the free or bound $(MTR)_2Mg^{2+}$ complexes in the 1:1 and 2:1 duplex complexes determined from the 5 ns dynamics simulation. Angle ϕ is subtended by atoms H1−C1−O−C3 while angle ψ is subtended by atoms C1−O−C3−H3. Atom O represents a glycosidic oxygen between two sugar residues, and atom C3 is replaced by C6 and C2 in angle DDA2-ϕ and DDA3-ϕ, respectively. The C3−H3 pair is replaced by C6−C5 and C2−H2 pair in torsion angles CHR−DDA2 and CHR−DDA3, respectively. The two MTR monomers in a $(MTR)_2Mg^{2+}$ complex are denoted respectively by I and II as shown in Figure 1. Two $(MTR)_2Mg^{2+}$ complexes in a 2:1 duplex complex are denoted respectively by MTR_2^{first} and MTR_2^{second} while an average value of the two $(MTR)_2Mg^{2+}$ complexes for the NMR set is denoted by MTR_2^{avg}.

monomers are symmetrically coordinated in the duplex complex (Figure 6a). However, monomers I and II are somewhat asymmetrically coordinated in the bound $(MTR)_2Mg^{2+}$ complex of the 1:1 or 2:1 duplex complexes as opposed to those symmetrically coordinated in the free $(MTR)_2Mg^{2+}$ complex (Figure 6b). The conformation of bound $(MTR)_2Mg^{2+}$ complexes is distorted significantly from that of the free one as revealed by difference in the glycosidic torsion angles measured between them. The glycosidic linkages of 1:1 duplex complexes are also different from those of the 2:1 duplex complexes, suggesting that the conformations of the sugar residues of the bound $(MTR)_2Mg^{2+}$ complex of the former are different from those of the latter. Moreover, the $(MTR)_2Mg^{2+}$ 1:1 duplex complex binds differently to the minor groove of the DNA duplex than the 2:1 duplex complex as revealed by the differences in the following glycosidic linkages, DDA3-ϕ(II), DDA3-ψ(I), DDL-ϕ(I), DDL-ψ(I), DDL-ψ(II), and MDA-ϕ(I) (Figures 1 and 6b). This corresponds to the conformational plasticity of the DDA3-DDL-MDA trisaccharide observed in the NMR study[19] plus the difference in recognition of the MDA sugar between the 1:1 and 2:1 duplex complexes by the DNA duplex. The MDA(I) sugar of the 1:1 duplex complex appears to extend to the A6 base through the plasticity of the glycosidic linkages, while that of the 2:1 duplex complex points inwardly to avoid a mutual clash between the two trisaccharide segments (Figures 6b and 7). The difference between the binding of one or two $(MTR)_2Mg^{2+}$ complexes with the DNA duplex to form either the 1:1 or 2:1 duplex complex results from the high conformational plasticity of the glycosidic linkages.

The difference in recognition of the MDA(I) sugar by the DNA duplex between the 1:1 and 2:1 duplex complexes is further elucidated in Figures 7a and 7b where patterns of hydrogen bond formation of both are compared. Formation of the hydrogen bonds between the N3 atom (acceptor) of the A6 base and the O2 atom (acceptor) of the T5 base with the OH3 atom (donor) of the MDA(I) sugar are detected respectively for the 1:1 and 2:1 duplex complexes (Figures 7a and 7b). A rare donor−acceptor pair with an occupancy of 0.38 is also detected between the OH3 atom of the MDA(I) segment and the O2 atom of the T5 base (Figure 7a and Table 2) for the 1:1 duplex complex. A comparison for patterns of hydrogen bond formation between the 1:1 and 2:1 duplex complexes during the 5 ns MD simulation is shown in Table 2. Except for the G3(NH_2-2e)−CHR(I)(OH8) donor−acceptor pair, most of these hydrogen bonds detected are different between the two duplex complexes (Table 2). This further shows that the binding between each of the $(MTR)_2Mg^{2+}$ 2:1 duplex complexes with the minor groove of the DNA duplex is symmetrical while that of the $(MTR)_2Mg^{2+}$ 1:1 duplex complex is somewhat extended (Figure 7). Note that helical rise at the G3−C4 step between the 1:1 and 2:1 duplex complexes is quite different (Figure 5a) although no apparent difference in variation of the minor groove widths between both bound duplexes up to the occupied half of the duplex is observed (Figure 5c). Moreover, there is no significant difference in the glycosidic linkages DDA3-ψ(II) and DDL-ϕ(II) between the 1:1 and 2:1 duplex complexes (Figure 6b) up to the step, and the corresponding trisaccharide chains of the $(MTR)_2Mg^{2+}$ complexes of both are slightly extended. However, the glycosidic linkages DDL-ψ(I) and MDA-ϕ(I) of the 1:1 duplex complex appear to be more extended (Figure 6b) such that a hydrogen bond between the N3 atom (acceptor) of the A6 base and the OH3 atom (donor) of the MDA(I) sugar of the duplex complex is formed (Figure 7a and Table 2).

The gas-phase energies, solvation free energies, and entropies for the free $(MTR)_2Mg^{2+}$ complex, the free DNA duplex, and the 1:1 and 2:1 duplex complexes were calculated from the MD simulation by MM/GB-SA[24] and normal-mode analysis and are presented in Tables 3 and 4, respectively. A stepwise binding mechanism where the first $(MTR)_2Mg^{2+}$ complex binds the free DNA duplex to form a 1:1 complex and then the second $(MTR)_2Mg^{2+}$ complex binds the 1:1 complex to form a 2:1 duplex complex (Figure 2) is assumed for computing the free energy. This binding procedure has been observed experimentally by Sastry et al.[19] by adding the $(MTR)_2Mg^{2+}$ complex gradually to the DNA duplex and was used by Harris et al.[22]

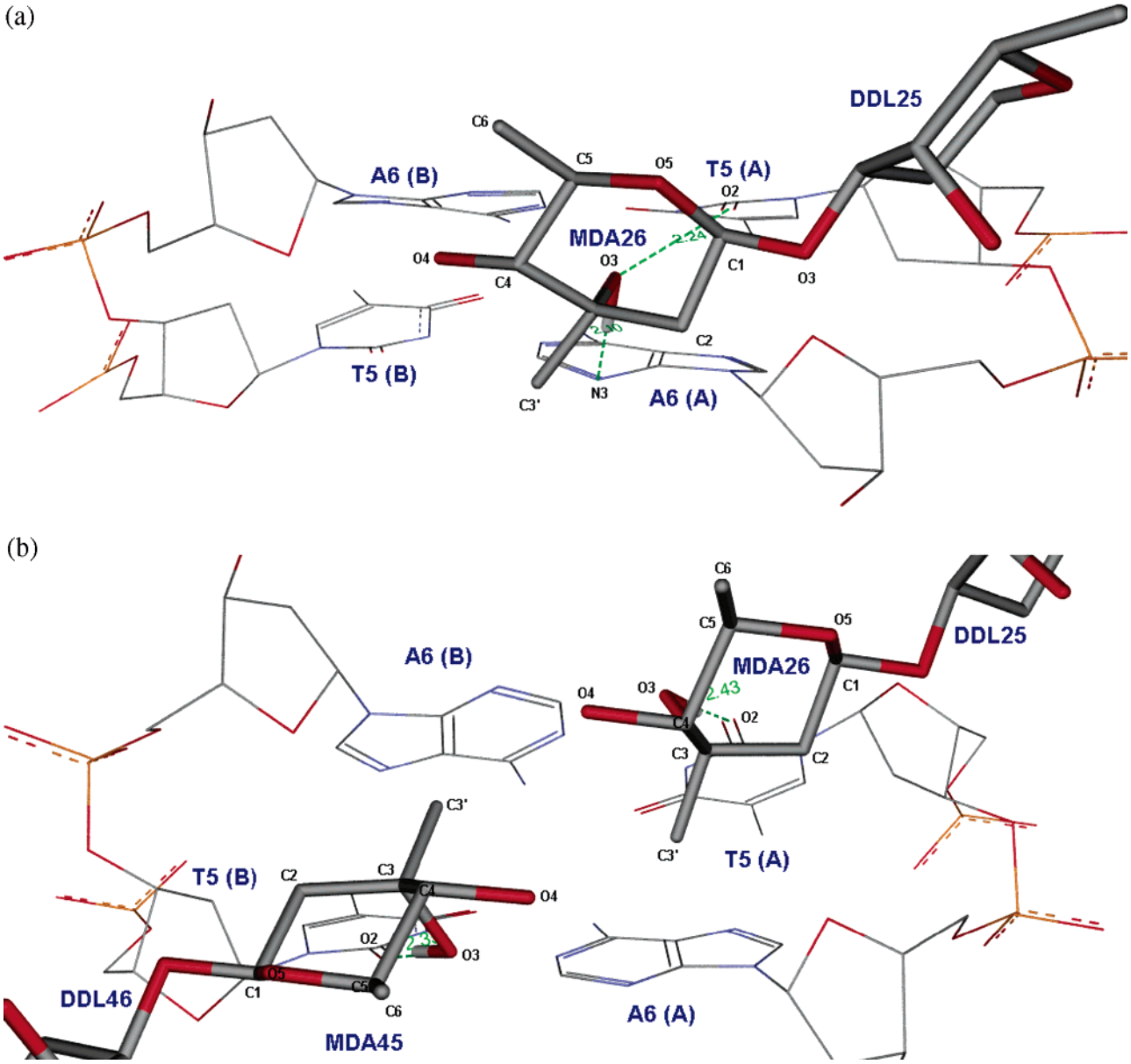

Figure 7. Some major interactions between the MDA residue of the MTR monomer (I) and the DNA duplex in the (a) 1:1 and (b) 2:1 duplex complexes determined from the time-averaged structures obtained from the MD simulation. The green dotted line represents a hydrogen bond between the ligand and the receptor and its length. The DNA residues of the different chains are abbreviated as T, A, G, and C with A or B behind.

TABLE 2: Hydrogen Bond Formation[a] between the $(MTR)_2Mg^{2+}$ Complex and the DNA Duplex Analyzed from the 5 ns MD Simulation for 1:1 and 2:1 Duplex Complexes

	1:1 complex			2:1 complex		
donor−acceptor	occupancy[b]	distance (Å)	angle (deg)	occupancy[b]	distance (Å)	angle (deg)
$G3(NH_2\text{-}2e)-CHR_I(OH8)$	96.67	2.97	163.98	96.89	2.97	160.32
$G7(NH_2\text{-}2e)-CHR_{II}(OH8)$	NA			97.27	2.96	160.07
$MDA_I(OH3)-T5(O2)$	0.38	3.08	144.27	98.90	2.80	170.05
$MDA_{II}(OH3)-A2(N3)$	1.20	2.91	168.15	96.86	2.88	169.40
$MDA_I(OH3)-A6(N3)$	99.06	2.83	164.64			

[a] A distance between the donor and the acceptor heteroatom of less than 3.3 Å as well as an angle of donor hydrogen−acceptor of larger than 135° is considered as a hydrogen bond. [b] Occupancy is in units of percentage of the investigated time period.

for computing the binding free energy for a drug with a 12-mer DNA duplex. The values computed for $T\Delta\Delta S$ at 300 K and $\Delta\Delta(E_{gas} + G_{sol})$ are respectively 1.80 and −4.00 kcal/mol, which give rise to a binding free energy $\Delta\Delta G$ of −5.8 kcal/mol (Tables 3 and 4) for the 2:1 duplex complex. This result agrees well with the experimentally measured one of −5.4 kcal/mol.[6] The binding free energy for the 1:1 duplex complex computed using the thermodynamic cycle described in Figure 2 is −15.09 kcal/mol (Table 3). In addition, the binding free energy change $\Delta(E_{gas} + G_{sol})$ was decomposed to components of contribution from the internal, van der Waals, sum of Coulomb and polar solvation, and nonpolar solvation free energy on a per-residue basis. Apparently, no significant changes occur in these energy terms for the unoccupied DNA residues. However, some significant changes in the van der Waals energy are found around the sugar recognition sites on the bound

TABLE 3: Binding Free Energy Components Calculated for the Free DNA to the 1:1 Drug−DNA Complex from Separate Trajectories[a]

	1:1 complex	free DNA	free MTR_2Mg^{2+}	Δ^e
contribution[b]	mean ± σ	mean ± σ	mean ± σ	mean ± σ
E_{elec}	−461.31 ± 0.75	307.52 ± 0.64	−482.82 ± 0.19	−286.01 ± 0.94
E_{vdw}	−179.01 ± 0.21	−166.52 ± 0.15	57.07 ± 0.12	−69.56 ± 0.29
E_{int}	1234.23 ± 0.35	934.11 ± 0.30	295.03 ± 0.19	5.09 ± 0.50
E_{gas}	593.92 ± 0.78	1075.12 ± 0.66	−130.72 ± 0.23	−350.48 ± 0.99
G_{np}	27.78 ± 0.00	22.38 ± 0.00	11.34 ± 0.00	−5.94 ± 0.00
G_{GB}	−4461.06 ± 0.68	−4593.29 ± 0.58	−169.66 ± 0.11	301.89 ± 0.83
G_{solv}	−4433.28 ± 0.68	−4570.91 ± 0.58	−158.33 ± 0.11	295.96 ± 0.83
$G_{gas+solv}$ [c]	−3839.36 ± 0.34	−3495.79 ± 0.29	−289.05 ± 0.20	−54.52 ± 0.48
TS_{total} [d]	717.69 ± 0.12	516.01 ± 0.21	241.11 ± 0.04	−39.43 ± 0.23
G_{total}	−4557.05 ± 0.36	−4011.80 ± 0.36	−530.16 ± 0.20	−15.09 ± 0.53

[a] All values are in kcal/mol ± standard error of mean values, for $T = 300$ K. [b] E_{gas} = Coulombic energy (E_{elec}) + van der Waals energy (E_{vdw}) + internal energy (E_{int}); G_{solv} = solvation free energy = nonpolar solvation free energy (G_{np}) + polar solvation free energy (G_{GB}); $G_{gas+solv} = E_{gas} + G_{solv}$; TS_{total} = total entropy contribution by summing up translational, rotational, and vibrational entropy determined by normal-mode analysis; $G_{total} = G_{gas+solv} - TS_{total}$. [c] Averaged over 4000 snapshots from the MD simulation (1.0−5.0 ns). [d] Averaged over 800 snapshots from the MD simulation (1.0−5.0 ns). [e] Contribution (1:1 complex) − contribution (free DNA) − contribution (free MTR_2Mg^{2+}).

TABLE 4: Binding Free Energy Components Calculated for the Free DNA to the 1:1 Drug−DNA Complex from Separate Trajectories[a]

	2:1 complex	1:1 complex	free MTR_2Mg^{2+}	Δ^e
contribution[b]	mean ± σ	mean ± σ	mean ± σ	mean ± σ
E_{elec}	−1048.82 ± 0.83	−461.31 ± 0.75	−482.82 ± 0.19	−104.70 ± 1.09
E_{vdw}	−195.38 ± 0.26	−179.01 ± 0.21	57.07 ± 0.12	−73.44 ± 0.37
E_{int}	1543.34 ± 0.41	1234.23 ± 0.35	295.03 ± 0.19	14.08 ± 0.57
E_{gas}	299.14 ± 0.86	593.92 ± 0.78	−130.72 ± 0.23	−164.06 ± 1.16
G_{np}	33.16 ± 0.00	27.78 ± 0.00	11.34 ± 0.00	−5.96 ± 0.00
G_{GB}	−4519.23 ± 0.75	−4461.06 ± 0.68	−169.66 ± 0.11	111.50 ± 0.98
G_{solv}	−4486.07 ± 0.75	−4433.28 ± 0.68	−158.33 ± 0.11	105.54 ± 0.98
$G_{gas+solv}$ [c]	−4186.93 ± 0.39	−3839.36 ± 0.34	−289.05 ± 0.20	−58.52 ± 0.56
TS_{total} [d]	921.17 ± 0.10	717.69 ± 0.12	241.11 ± 0.04	−37.63 ± 0.17
G_{total}	−5108.10 ± 0.40	−4557.05 ± 0.36	−530.16 ± 0.20	−20.89 ± 0.99
$\Delta\Delta(E_{gas} + G_{solv})$[f]				−4.00 ± 0.74
$T\Delta\Delta S$[f]				1.80 ± 0.29

[a–d] See legend of Table 3. [e] Contribution (2:1 complex) − contribution (1:1 complex) − contribution (free MTR_2Mg^{2+}). [f] Contribution (2:1 complex) + contribution (free DNA) − 2·contribution (1:1 complex); see caption of Figure 2 for details.

TABLE 5: Configurational Entropies of the First and Second Half of the DNA Duplex Alone Computed for the Free DNA Duplex and the 1:1 and 2:1 Duplex Complexes[a]

	$DNA^{first\ half}$		$DNA^{second\ half}$	
system	TS	$T\Delta S$	TS	$T\Delta S$
free DNA	450.00		449.28	
		−16.75		2.22
1:1 complex	433.25		451.50	
		−15.22		−35.85
2:1 complex	418.03		415.65	

[a] All values are calculated from the MD snapshots as described in the legend of Table 1. The configurational entropies are calculated by quasiharmonic normal-mode analysis.

duplex, namely, the specific GC binding and central TA sites. Similar changes are also found on the counterparts of the bound ligand, namely, at residues CHR and MDA where formation of hydrogen bonds with the duplex is detected (Figures 7a and 7b). The minor groove appears to be widened somewhat such that the steric hindrance on the incoming CHR and sugar residues of the bound ligand is reduced substantially.

A comparison for the entropies computed for the free and bound DNA duplexes in the 1:1 and 2:1 duplex complexes using the quasiharmonic normal-mode analysis on the MD simulation data is presented in Table 5. The quasiharmonic normal-mode analysis is somewhat different from the normal-mode one employed to estimate the vibrational entropy for each molecular species because the anharmonic terms in the potentials due to the solvent effects are included by the former. The entropies computed for the two halves of the free DNA duplex are very similar and so are for those of the bound DNA duplex of the 2:1 duplex complex, indicating that the length of the MD simulation is sufficient for the analysis (Table 5). The binding of a $(MTR)_2Mg^{2+}$ complex with the DNA duplex in a 1:1 duplex complex appears to stabilize the occupied but not the unoccupied half of the duplex since while the corresponding entropy computed for the former is reduced substantially while that for the latter is not (Table 5). This is also reflected in the huge variations in minor groove width detected for the central T5−A6 and A6−T5 base pairs of the DNA duplex in a 1:1 duplex complex (Figure 5c). The conformational freedom of both halves of the DNA duplex is further restricted to nearly the same extent once a second $(MTR)_2Mg^{2+}$ complex is bound (Table 5). The conformational flexibility of the free and bound DNA duplex in the 1:1 and 2:1 duplex complexes is also compared using the analysis results from the PTRAJ8 module. The groove width variation of each DNA duplex is plotted as a function of the top eigenvector computed from the trajectories of the MD simulation as shown in Figure 8. The free DNA duplex behaves like a string, and the corresponding vibration modes on one site are freely transferred to the other one (Figure 8). While negligible harmonics are detected for a 2:1 duplex complex, a remarkable and asymmetric one is seen for the unoccupied site of a 1:1 duplex complex (Figure 8). This corresponds to the fact that the unoccupied site of a 1:1 duplex is still considerably flexible and similar to the same part of free DNA duplex (Table 5). Therefore, binding of the second $(MTR)_2Mg^{2+}$ complex with

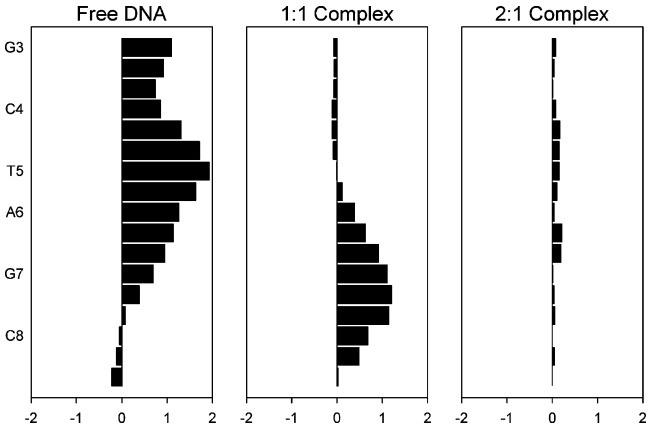

Figure 8. Harmonic modes corresponding to the groove width variation (in Å) are computed using the top eigenvectors obtained from analyses of the MD trajectories for the free DNA duplex plus the 1:1 and 2:1 duplex complexes.

TABLE 6: Configurational Entropies of $(MTR)_2Mg^{2+}$ Alone Computed for the $(MTR)_2Mg^{2+}$ 1:1 and 2:1 Duplex Complexes[a]

	$(MTR)_2Mg^{2+}$	
system	TS	$T\Delta S$
free $(MTR)_2Mg^{2+}$	450.04	
		−25.29
1:1 complex	424.75	
		−4.58
2:1 complex[b]	420.17	

[a] All values are calculated from the MD snapshots as described in the legend of Table 1. The configurational entropies are calculated by quasiharmonic normal-mode analysis. [b] Averaged values of 420.84 and 419.50 from two $(MTR)_2Mg^{2+}$ complexes.

a 1:1 duplex complex appears to be not guided by the first bound $(MTR)_2Mg^{2+}$ complex. Moreover, the conformational freedom of the bound $(MTR)_2Mg^{2+}$ complex is gradually reduced from that in free complex to that in 2:1 duplex complex (Table 6).

Conclusion

Our MD simulation results show that the binding of two $(MTR)_2Mg^{2+}$ complexes with each being coordinated by a Mg^{2+} ion with the 10-mer DNA duplex is a somewhat anticooperative event, which agrees with that observed experimentally by Sastry et al.[19] The minor groove in the central part of the 1:1 or 2:1 duplex complex is apparently widened during the drug binding process. For the formation of a 2:1 duplex complex, the sugar residues of both $(MTR)_2Mg^{2+}$ complexes interact with the T5 base to form some hydrogen bonds, which then distort the DNA duplex. These sugar residues also interact with the A6 base and then widen the central minor groove of the DNA duplex. Widening of the minor groove permits the interaction between both trisaccharide chains and central T5−A6/A6−T5 base steps and the formation of some essential hydrogen bonds between them. Binding of one $(MTR)_2Mg^{2+}$ complex with the DNA duplex to form a 1:1 duplex complex does not restrict the conformational flexibility of the unoccupied site as revealed by the configurational entropies computed. The bound $(MTR)_2Mg^{2+}$ complex in a 1:1 duplex complex appears to be less flexible and causes some changes of the conformation of the bound DNA duplex.

Except similar binding between the central CHR segment and the specific G3 base observed, the MDA sugar of the 1:1 duplex complex binds with A6 while those of the 2:1 duplex complex bind with either the T5 or the A2 base. The enthalpy of binding by the first and then second $(MTR)_2Mg^{2+}$ complex with the corresponding sites on the DNA duplex are respectively −54.52 and −58.52 kcal/mol (Tables 3 and 4), which are far larger than those reported by Harris et al.[22] for binding of the drug Hoechst 33258 with a 12-mer duplex. There is also a substantial difference between our system and that of Harris et al.[22] in the entropy computed for the second half of the duplex upon binding with the second drug complex. A much larger entropic penalty is computed here (Table 5) for binding of the second drug complex with the second half of the duplex than that reported by Harris et al.[22] for their system. In fact, an apparent increase in entropy of the first half bound duplex is observed[22] upon binding of the free second half duplex with the drug complex. The conformational freedom of the second half is further reduced upon binding with the second drug complex although a message is being passed back to the first occupied site that results in an increase in its configurational entropy.[22] On the contrary, the conformational freedom of the free second half duplex of our system is not restricted upon binding with a drug complex by the first half (Table 5), unlike that reported for the Hoechst 33258 system.[22] The minor groove width of the free second half of the 1:1 duplex complex appears to be shrunk, and the twist is being lengthened somewhat upon binding with a $(MTR)_2Mg^{2+}$ complex at the first half of the duplex. This reveals that the conformation of the unoccupied site especially at the G7−C8 bases is more or less like B-DNA. Furthermore, while no apparent harmonics for the bound first half are present, an evident one is observed for the free second half of the 1:1 duplex complex (Figure 8). This indicates that a subsequent binding by the second $(MTR)_2Mg^{2+}$ complex with the unoccupied site of a 1:1 complex to form a 2:1 duplex complex is possible, though the binding of a much larger drug complex presented in this study with the DNA duplex appears to be in an anticooperative manner.

Acknowledgment. This work is supported in part by the National Science Council, Taiwan (Grant No. NSC92-2313-B007-002). The AMBER 7.0, PTRAJ 8.0, and GAUSSIAN98[34] siumlations used in this study were conducted at the National Center for High Performance Computing, Taiwan.

Supporting Information Available: Force field parameters used for the MTR dimer and figure showing the decomposition of the binding free energy. This material is available free of charge via the Internet at http://pubs.acs.org

References and Notes

(1) Yarbo, J. W.; Kennedy, B. J.; Barnum, C. P. *Cancer Res.* **1968**, *26*, 36.
(2) Miller, D. M.; Polansky, D. A.; Thomas, S. D.; Ray, R.; Campbell, V. W.; Sanchez, J.; Koller, C. A. *Am. J. Med. Sci.* **1987**, *294*, 388.
(3) Koller, C. A.; Miller, D. M. *N. Engl. J. Med.* **1986**, *315*, 1433.
(4) Koller, C. A.; Campbell, V. W.; Yang, A.; Mulhern, A.; Miller, D. M. *J. Clin. Invest.* **1985**, *76*, 365.
(5) Miller, D. M.; Baker, V.; Thomas, S.; Rigsby, D.; Sanchez, J. D.; Koller, C. A. *Blood* **1986**, *68*, 260a.
(6) Chakrabarti, S.; Bhattacharyya, B.; Dasgupta, D. *J. Phys. Chem. B* **2002**, *106*, 6947.
(7) Berveridge, D. L.; McConnell, K. J. *Curr. Opin. Struct. Biol.* **2000**, *10*, 182.
(8) Cheatham, T. E., III; Kollman, P. A. *Annu. Rev. Phys. Chem.* **2000**, *51*, 435.
(9) Aich, P.; Dasgupta, D. *Biochem. Biophys. Res. Commun.* **1990**, *173*, 689.
(10) Aich, P.; Sen, R.; Dasgupta D. *Chem.−Biol. Interact.* **1992**, *83*, 23.
(11) Aich, P.; Sen, R.; Dasgupta, D. *Biochemistry* **1992**, *31*, 2988.
(12) Aich, P.; Dasgupta, D. *Biochemistry* **1995**, *34*, 1376.

(13) Chakrabarti, S.; Mir, M. A.; Dasgupta, D. *Biopolymers* **2001**, *62*, 131.

(14) Banville, D. L.; Keniry, M. A.; Shafer, R. H. *Biochemistry* **1990**, *29*, 6521.

(15) Banville, D. L.; Keniry, M. A.; Shafer, R. H. *Biochemistry* **1990**, *29*, 9294.

(16) Gao, X.; Patel, D. J. *Biochemistry* **1989**, *28*, 751.

(17) Sastry, M.; Patel, D. J. *Biochemistry* **1993**, *32*, 6588.

(18) Majee, S.; Sen, R.; Guha, S.; Bhattacharyya, D.; Dasgupta, D. *Biochemistry* **1997**, *36*, 2291.

(19) Sastry, M.; Fiala, R.; Patel, D. J. *J. Mol. Biol*. **1995**, *251*, 674.

(20) Zimmer, C.; Wahnert, U. *Prog. Biophys. Mol. Biol.* **1986**, *47*, 31.

(21) Boehncke, K.; Nonella, M.; Schulten, K. *Biochemistry* **1991**, *30*, 5465.

(22) Harris, Sarah A.; Gavathiotis, Evripidis; Searle, Mark S.; Orozco, Modesto; Laughton, Charles A. *J. Am. Chem. Soc*. **2001**, *123*, 12658.

(23) Gao, X.; Patel, D. J. *Biochemistry* **1990**, *29*, 10940.

(24) Tsui, V.; Case, D. A. *Biopolymers* **2001**, *56*, 275.

(25) Case, D. A.; Pearlman, D. A.; Caldwell, J. W.; Cheatham, T. E., III; Wang, J.; Ross, W. S.; Simmerling, C. L.; Darden, T. A.; Merz, K. M.; Stanton, R. V.; Cheng, A. L.; Vincent, J. J.; Crowley, M.; Tsui, V.; Gohlke, H.; Radmer, R. J.; Duan, Y.; Pitera, J.; Massova, I.; Seibel, G. L.; Singh, U. C.; Weiner, P. K.; Kollman, P. A.; University of California: San Francisco, 2002. *AMBER*, version 7.

(26) Wang, Junmei; Cieplak, Piotr; Kollman, Peter A. *J. Comput. Chem.* **2000**, *21*, 1049.

(27) Jorgensen, W. L.; Chandrasekhar, J.; Madura, J.; Impley, R. W.; Klein, M. L. *J. Chem. Phys.* **1983**, *79*, 926.

(28) Bayly, C. I.; Cieplak, P.; Cornell, W. D.; Kollman, P. A. *J. Phys. Chem*. **1993**, *97*, 10269.

(29) Pathiaseril A.; Woods, R. J. *J. Am. Chem. Soc*. **2000**, *122*, 331.

(30) Darden, T.; York, D.; Pedersen, L. *J. Chem. Phys*. **1993**, *98*, 10089.

(31) Ryckaert, J. P.; Ciccotti, G.; Berendsen, H. J. C. *J. Comput. Phys*. **1977**, *23*, 237.

(32) Lavery, R.; Sklenar, H. *J. Biomol. Struct. Dyn*. **1989**, *6*, 63.

(33) McQuarrie, D. A. *Statistical Mechanics*; Harper and Row: New York, 1976.

(34) Frisch, M. J.; Trucks, G. W.; Schlegel, H. B.; Scuseria, G. E.; Robb, M. A.; Cheeseman, J. R.; Zakrzewski, V. G.; Montgomery, J. A., Jr.; Stratmann, R. E.; Burant, J. C.; Dapprich, S.; Millam, J. M.; Daniels, A. D.; Kudin, K. N.; Strain, M. C.; Farkas, O.; Tomasi, J.; Barone, V.; Cossi, M.; Cammi, R.; Mennucci, B.; Pomelli, C.; Adamo, C.; Clifford, S.; Ochterski, J.; Petersson, G. A.; Ayala, P. Y.; Cui, Q.; Morokuma, K.; Malick, D. K.; Rabuck, A. D.; Raghavachari, K.; Foresman, J. B.; Cioslowski, J.; Ortiz, J. V.; Stefanov, B. B.; Liu, G.; Liashenko, A.; Piskorz, P.; Komaromi, I.; Gomperts, R.; Martin, R. L.; Fox, D. J.; Keith, T.; Al-Laham, M. A.; Peng, C. Y.; Nanayakkara, A.; Gonzalez, C.; Challacombe, M.; Gill, P. M. W.; Johnson, B. G.; Chen, W.; Wong, M. W.; Andres, J. L.; Head-Gordon, M.; Replogle, E. S.; Pople, J. A. *Gaussian 98*, revision A11.3; Gaussian, Inc.: Pittsburgh, PA, 1998.